Inorganic Chemistry
Article
Cite This: Inorg. Chem. 2018, 57, 9531−9537
pubs.acs.org/IC

Synthesis, Crystal Structure, and Optical Gap of Two-Dimensional Halide Solid Solutions $CsPb_2(Cl_{1-x}Br_x)_5$

Yibao Chen,[†] Maxim S. Molokeev,[‡,§,⊥] Victor V. Atuchin,[¶,∥,#] Ali H. Reshak,[▽,◆] Sushil Auluck,[○] Zeyad A. Alahmed,[◆] and Zhiguo Xia*[,†]

[†]The Beijing Municipal Key Laboratory of New Energy Materials and Technologies, School of Materials Sciences and Engineering, University of Science and Technology Beijing, Beijing 100083, P. R. China

[‡]Laboratory of Crystal Physics, Kirensky Institute of Physics, Federal Research Center, Krasnoyarsk Scientific Center, Siberian Branch of the Russian Academy of Sciences, Krasnoyarsk 660036, Russia

[§]Siberian Federal University, Krasnoyarsk 660041, Russia

[⊥]Department of Physics, Far Eastern State Transport University, Khabarovsk 680021 Russia

[¶]Laboratory of Optical Materials and Structures, Institute of Semiconductor Physics, Siberian Branch of the Russian Academy of Sciences, Novosibirsk 630090, Russia

[∥]Functional Electronics Laboratory, Tomsk State University, Tomsk 634050, Russia

[#]Laboratory of Single Crystal Growth, South Ural State University, Chelyabinsk 454080, Russia

[▽]New Technologies Research Centre, University of West Bohemia, Univerzitni 8, Pilsen 30614, Czech Republic

[○]National Physical Laboratory, Council of Scientific and Industrial Research, Dr. K. S. Krishnan Marg, New Delhi 110012, India

[◆]Department of Physics and Astronomy, College of Science, King Saud University, P.O. Box 2455, Riyadh 11451, Saudi Arabia

Supporting Information

ABSTRACT: Exploring new perovskite-related solid-state materials and the investigating composition-dependent structural and physical properties are highly important for advanced functional material development. Herein, we present the successful hydrothermal synthesis of tetragonal $CsPb_2Cl_5$ and the anion-exchange phase formation of $CsPb_2(Cl_{1-x}Br_x)_5$ (x = 0−1) solid solutions. The $CsPb_2(Cl_{1-x}Br_x)_5$ crystal structures, which crystallize in the tetragonal system, space group $I4/mcm$, with parameters similar to those of $CsPb_2Cl_5$, have been determined by Rietveld analysis. The optical band gap was obtained by UV−vis spectroscopy, and the band structure was further calculated by the full-potential method within the generalized gradient approximation. It was revealed that the band gap in $CsPb_2(Cl_{1-x}Br_x)_5$ solid solutions can be tuned over the range of 4.5−3.8 eV by anion substitution.

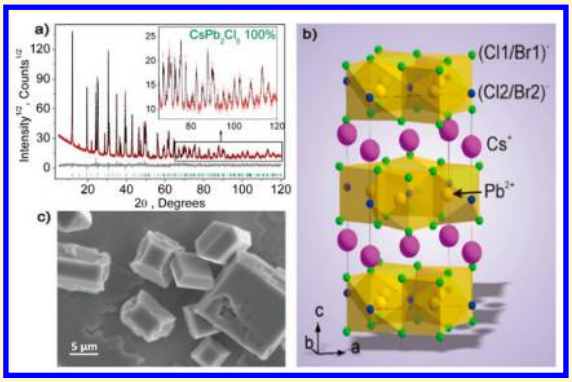

INTRODUCTION

The discovery of new solid-state materials for emerging applications is extremely important, and many crystals with such specific characteristics as nonlinear-optical properties, wide transparency range, low compressibility, negative thermal expansion, photoluminescence properties, and promising electronic and magnetic parameters were designed and evaluated in the past few years.[1−11] Recently, inorganic lead halide perovskite-related compounds have become promising functional materials for optoelectronic applications because of their remarkable spectroscopic and electronic properties, including tunable band gap and appropriate chemical stability.[12−16] Earlier, cesium lead halides and other closely related compounds were obtained in the macroscopic forms of thin films, powders, and bulk crystals using different technological approaches, and many key physical properties were measured, which yields a basis for a wide comparison and selection of optimal materials for use at a nanoscale.[17−22] Intrinsically, the specific physical properties of lead halides originate from the PbX_6 basic functional units existing in the perovskite-related crystals. From a structural point of view, on the basis of the PbX_6 octahedra connection, the lead perovskite dimensionality was classified into zero-dimensional (0D), two-dimensional (2D), and three-dimensional (3D) structures. Colloidal quasi-2D semiconductor nanoplatelets are an interesting type of nanocrystal because of their unique spectroscopic properties, such as increased exciton binding

Received: June 7, 2018
Published: July 16, 2018

DOI: 10.1021/acs.inorgchem.8b01572
Inorg. Chem. 2018, 57, 9531−9537

energies, reduced fluorescence decay times, and notable optical nonlinearity.[23] Therefore, there are intensive investigations on the metal halides with perovskite or close-to-perovskite structures as attractive semiconductors. Among them, perovskite-related metal halide colloidal nanoplatelets are an important type of nanomaterials because they not only enrich the diversity of the available semiconducting nanomaterials, but also potentially possess a platform for exploring new photophysical properties of 2D semiconducting materials.

The present study is aimed at the hydrothermal synthesis of solid solutions $CsPb_2(Cl_{1-x}Br_x)_5$ (x = 0, 0.2, 0.4, 0.6, 0.8, and 1) and evaluation of their electronic and optical parameters as a function of the Cl/Br ratio. It should be pointed out that the end compound $CsPb_2Br_5$ is actively used in modern photonic structures.[24−27] First, the compound $CsPb_2Cl_5$ was prepared by the ion-exchange reaction between $Cs_2PbCl_2(NO_3)_2$ and NaCl (or KCl) in an aqueous solution, and the tetragonal crystal structure was determined in space group $I4/mcm$.[28] The 2D structure is formed by the layers of $PbCl_4$ tetrahedra, and Cs^+ ions are positioned between the layers. To our best knowledge, information about the crystal structure of related bromide $CsPb_2Br_5$ is absent in the literature, although the $CsPb_2Br_5$ cell parameters were reported recently.[29] On the basis of the available structural information shown in Table S1,[18,29−36] the same structure type can be reasonably assumed for $CsPbCl_5$ and $CsPbBr_5$. The wide-range tuning of the physical properties could be possible in $CsPb_2(Cl_{1-x}Br_x)_5$ solid solutions without phase transition singularities.

As of now, three structural types are known for lead halides with the general composition APb_2X_5 (A = Ag, NH_4, K, Rb, Cs, Tl; X = Cl, Br, I), and the available structural parameters are summarized in Table S1. The specific monoclinic structure was reported for $AgPb_2Br_5$, which is the only known Ag-containing compound with the composition APb_2X_5[30]. The most numerous set of monoclinic compounds includes KPb_2Cl_5, KPb_2Br_5, $K_{0.94}Tl_{0.06}Pb_2Cl_{4.87}Br_{0.13}$, $NH_4Pb_2Cl_5$, $Tl_{0.86}K_{0.14}Pb_2Cl_5$, $Tl_{0.96}K_{0.04}Pb_2Cl_{4.82}Br_{0.18}$, and $TlPb_2Cl_5$, and this family was actively evaluated in the past.[18,28,31,33,35] The compounds $RbPb_2Br_5$, $CsPb_2Cl_5$, $CsPb_2Br_5$, and $InPb_2I_5$ possess similar tetragonal structures, and the existence of the wide-range solid solutions $(Rb,Cs)Pb_2Br_5$ and $CsPb_2(Cl,Br)_5$ seems to be possible. However, anion substitution in $CsPb_2(Cl,Br)_5$ solid solutions provides giant variations of the unit cell volume, and this is an indicator of strong variations of the electronic structure and optical characteristics on the transformation from $CsPb_2Cl_5$ to $CsPb_2Br_5$ (Table S1). Therefore, in this study, the crystal structures of $CsPb_2(Cl_{1-x}Br_x)_5$ (x = 0, 0.2, 0.4, 0.6, 0.8, and 1) were defined by Rietveld analysis. The compounds crystallize in the tetragonal system, space group $I4/mcm$, with the unit cell parameters close to those of $CsPb_2Cl_5$. Their optical band gaps were determined by UV−vis spectroscopy, and the band structures were further calculated by the full-potential method within the generalized gradient approximation (GGA).

EXPERIMENTAL SECTION

Materials and Synthesis. All starting reagents were used without any additional purification: Cesium chloride (CsCl, 99.99%) and lead chloride ($PbCl_2$; analytical reagent) were purchased from Shanghai Aladdin Biochemical Technology Co., Ltd. Hydrogen chloride (HCl; 38%) and hydrobromic acid (HBr; 48%) were purchased from Beijing Chemical Works. The $CsPb_2(Cl_{1-x}Br_x)_5$ solid solutions were synthesized through the hydrothermal method in a haloid acid solution at different HCl/HBr ratios. Thus, 0.75 mmol of $PbCl_2$ and 0.75 mmol of CsCl were placed in a poly(tetrafluoroethylene) (PTFE) reactor, and, subsequently, a mixture of HCl (5 mL for $CsPb_2Cl_5$, 4 mL for $CsPb_2Cl_4Br$, 3 mL for $CsPb_2Cl_3Br_2$, 2 mL for $CsPb_2Cl_2Br_3$, 1 mL for $CsPb_2ClBr_4$, and 0 mL for $CsPb_2Br_5$), HBr (0 mL for $CsPb_2Cl_5$, 1 mL for $CsPb_2Cl_4Br$, 2 mL for $CsPb_2Cl_3Br_2$, 3 mL for $CsPb_2Cl_2Br_3$, 4 mL for $CsPb_2ClBr_4$, and 5 mL for $CsPb_2Br_5$) and 10 mL of deionized water was slowly added to the PTFE reactor. After the hydrothermal reaction at 453 K for 24 h, the temperature was naturally decreased to room temperature, and the final powder product was filtered and finally dried at 373 K under vacuum.

Characterization. Powder X-ray diffraction (XRD) measurements were carried out using a D8 Advance diffractometer (Bruker, Germany) operating at 40 kV and a current of 40 mA with Cu Kα radiation (λ = 1.5406 Å). When the XRD patterns were measured for phase composition analysis, the scanning rate was 4°/min. For Rietveld analysis, the powder XRD patterns were collected using the same device, but, in this case, the 2θ step size was 0.013° and the counting time was as high as 1 s/step. The Rietveld refinement was performed using the package *TOPAS 4.2*.[37] The morphology and crystallite size of the $CsPb_2(Cl_{1-x}Br_x)_5$ samples were observed with the help of scanning electron microscopy (SEM; JEOL JSM-6510). The diffuse-reflectance spectra were recorded at room temperature using a Varian Cary 5 spectrophotometer over the UV−vis−near-infrared range.

Computational Methods. To investigate the ground-state properties of the $CsPb_2(Cl_{1-x}Br_x)_5$ compounds, first-principle calculations were implemented using the full-potential method (*Wien2k* code[38]) in the GGA [Perdew−Burke−Ernzerhof (PBE/GGA)] to optimize the available cell parameters and atomic positions. The Becke−Johnson potential[39] was applied to evaluate the ground-state properties in the relaxed structures of the $CsPb_2(Cl_{1-x}Br_x)_5$ compounds. The following parameters were used in the ab initio calculations: in the interstitial region, the basis functions were expanded up to $RMTK_{max}$ = 7.0 and inside the atomic spheres for the wave function. l_{max} = 10. The charge density was Fourier-expanded up to G_{max} = 12 (atomic units, au)$^{-1}$. In the irreducible Brillouin zone (IBZ), the self-consistency was obtained using 1000 $\vec{k}$ points. The self-consistent calculations were converged because the system total energy was stable within 0.00001 Ry. The electronic properties were calculated using 5000 $\vec{k}$ points over the IBZ. The input parameters required for calculating the total and partial density of states (TDOS and PDOS) were the energy eigenvalues and eigenfunctions, which were the natural outputs of a band-structure calculation. Thus, from the band-structure calculation, the PDOS and TDOS were obtained by the modified tetrahedron method.[40]

RESULTS AND DISCUSSION

Micromorphology and Structure Characterization. The XRD pattern recorded for $CsPb_2Cl_5$ is shown in Figure 1. This complex halide crystallizes in the tetragonal structure in space group $I4/mcm$. The XRD patterns obtained for the Br-containing compounds with the $CsPb_2(Cl_{1-x}Br_x)_5$ (x = 0.2, 0.4, 0.6, 0.8, and 1) compositions are very similar to that of $CsPb_2Cl_5$ and, respectively, the same structure type can be considered for all crystals. The crystal structures of all samples $CsPb_2(Cl_{1-x}Br_x)_5$ were obtained by Rietveld analysis, and the related information can be found in Figure S1 and Tables S2 and S3. The main parameters of the refinements are summarized in Table 1. The updated CIFs of $CsPb_2(Cl_{1-x}Br_x)_5$ (x = 0.2, 0.4, 0.6, 0.8, and 1) are available through CSD. Then, it is interesting to compare the cell parameters determined for $CsPb_2Cl_5$ and $CsPb_2Br_5$ to the available literature data listed in Table S1. As to $CsPb_2Cl_5$, the cell parameters determined in the present study are considerably bigger than those reported earlier.[17] However, as to $CsPb_2Br_5$, the parameter a refined in the present study is

DOI: 10.1021/acs.inorgchem.8b01572
Inorg. Chem. 2018, 57, 9531−9537

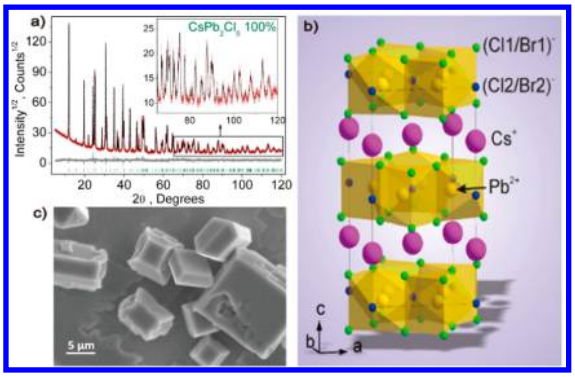

Figure 1. (a) Measured (black), calculated (red), and difference (gray) XRD patterns of the $CsPb_2Cl_5$ sample. (b) Crystal structure of $CsPb_2(Cl_{1-x}Br_x)_5$ halides. (c) SEM image of $CsPb_2Cl_5$ microcrystals.

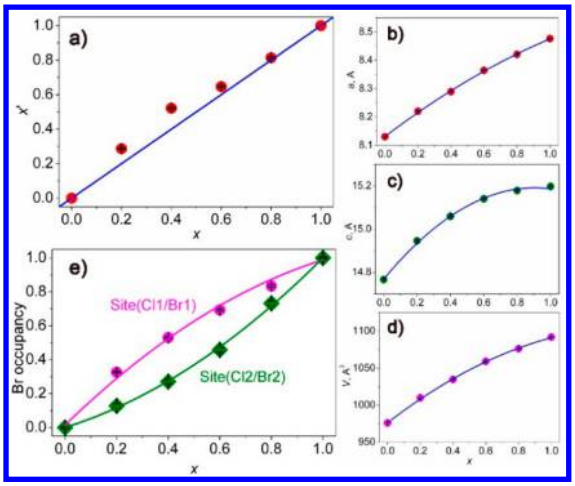

Figure 2. (a) Refined values x' (red circles) of the Br concentration in the samples per nominal x levels. Cell parameters (b) a and (c) c and (d) cell volume V dependent on x. (e) Occupancy values for Br^- in two anion sites in $CsPb_2(Cl_{1-x}Br_x)_5$ (x = 0, 0.2, 0.4, 0.6, 0.8, and 1).

significantly lower than that obtained in ref 29. Supposedly, the cell parameters are very sensitive to the real defect structure of the crystals. Besides, it should be mentioned that the value a = 6.002 Å earlier obtained for $CsPb_2Br_5$ in ref 41 is evidently wrong.

The typical $CsPb_2(Cl_{1-x}Br_x)_5$ structure is depicted in Figure 1b. This is a 2D structure with Cs^+ cations between the Pb^{2+} polyhedron layers. The Pb^{2+} coordination by halogen ions is not trivial. As a representative example, the $CsPb_2Cl_5$ structure can be considered by the bond-valence method.[42] Indeed, the bond valence sum calculated for the bond lengths d(Pb−Cl) in the range of 2.740(2)−3.222(2) Å is equal to 2.28, which is close to the 2+ formal valence state of the Pb^{2+} ion. Therefore, in order to build a $PbCl_n$ polyhedron, we should take all d(Pb−Cl) bonds in the range of 2.740(2)−3.222(2) Å, and such a construction leads to the bicapped trigonal prism $PbCl_8$ instead of the tetrahedron $PbCl_4$ mentioned elsewhere.[28] The bond valence sum for the four short d(Pb−O) bond lengths gave only the value of 1.66. The $CsPb_2Cl_5$ morphology evaluated by SEM is shown in Figure 1c. The low-resolution SEM images demonstrate the nearly uniform distribution of the particle sizes. The powder sample contains well-faceted nonagglomerated tetragonal particles with a side length of 5−10 μm and a thickness of 2−5 μm. Commonly, the presence of well-faceted microcrystal shapes is a robust indicator of a high structural quality of the powder samples, and this general relationship is evidently valid for the $CsPb_2(Cl_{1-x}Br_x)_5$ samples synthesized in the present study.[43−45]

The chemical formulas obtained from the Rietveld refinement can be written as $CsPb_2Cl_5$, $CsPb_2Cl_{3.57(2)}Br_{1.43(2)}$, $CsPb_2Cl_{2.39(2)}Br_{2.61(2)}$, $CsPb_2Cl_{1.77(2)}Br_{3.23(2)}$, $CsPb_2Cl_{0.93(2)}Br_{4.07(2)}$, and $CsPb_2Br_5$, which are close to the nominal compositions controlled by the HCl/HBr ratio in the synthesis. The refined values of the Br concentration x' per suggested nominal x values can be observed in Figure 2a. One can see that the deviation from the ideal linear function $x' = x$ is small, and it can be concluded that the desired compounds were obtained. Moreover, the cell parameters and cell volume increases with increasing x, as can be seen in Figure 2b−d, also prove the solid solution formation because the ion radius of Cl^- is smaller than that of Br^-.

The refined values of Br^- occupancies in the two anion sites Cl1/Br1 and Cl2/Br2 are different, as shown in Figure 2e. It is evident that the Cl1 site is preferable for the Br^- ion incorporation in comparison to the Cl2 site. This effect can be explained by the bigger average bond length d(Cl1/Br1−Pb/Cs) = 3.32 Å than d(Cl1/Br1−Pb/Cs) = 3.25 Å in the initial $CsPb_2Cl_5$ compound, and the Br^- ion prefers a bigger cage. However, because the difference between these average bond lengths is not very big, Br^- ions partly substitute Cl^- in both anion sites. To confirm the elemental uniformity of $CsPb_2(Cl_{1-x}Br_x)_5$, the Cs, Pb, Br, and Cl element maps for selected regions of the $CsPb_2Cl_5$, $CsPb_2Cl_2Br_3$, and $CsPb_2Br_5$ samples were recorded, and the patterns are shown in Figure 3. It can be seen that the constituent element distributions are uniform over the crystal area for all three selected samples with different chemical compositions.

In order to investigate the optical band-gap behavior, the UV−vis diffuse-reflectance spectra of $CsPb_2(Cl_{1-x}Br_x)_5$ were determined (Figure 4a). The band gaps of the $CsPb_2(Cl_{1-x}Br_x)_5$ compounds can be estimated using the equation[46]

$$[F(R_\infty)h\nu]^n = A(h\nu - E_g) \quad (1)$$

where $h\nu$ is the photon energy, A is a constant, E_g is the band gap, n = 2 for a direct transition and $^1/_2$ for an indirect

Table 1. Main Parameters of the Processing and Refinement of $CsPb_2(Cl_{1-x}Br_x)_5$ Samples with x = 0, 0.2, 0.4, 0.6, 0.8, and 1

x	x' (refined Br content)	space group	cell parameters (Å), cell volume (Å^3)	R_{wp}, R_p, R_B (%), χ^2
0	0	$I4/mcm$	a = 8.13020(8), c = 14.7666(2), V = 976.07(2)	7.17, 5.47, 3.17, 1.40
0.2	0.287(5)	$I4/mcm$	a = 8.2201(2), c = 14.9462(4), V = 1009.92(5)	5.89, 4.61, 1.49, 1.28
0.4	0.522(5)	$I4/mcm$	a = 8.2894(1), c = 15.0595(3), V = 1034.79(4)	6.82, 5.21, 2.74, 1.35
0.6	0.646(6)	$I4/mcm$	a = 8.3643(2), c = 15.1404(4), V = 1059.25(6)	7.98, 6.13, 3.51, 1.39
0.8	0.814(6)	$I4/mcm$	a = 8.4207(2), c = 15.1785(4), V = 1076.28(6)	7.93, 6.14, 3.78, 1.36
1	1	$I4/mcm$	a = 8.4765(3), c = 15.1974(6), V = 1091.95(8)	6.10, 4.68, 3.04, 1.86

DOI: 10.1021/acs.inorgchem.8b01572
Inorg. Chem. 2018, 57, 9531−9537

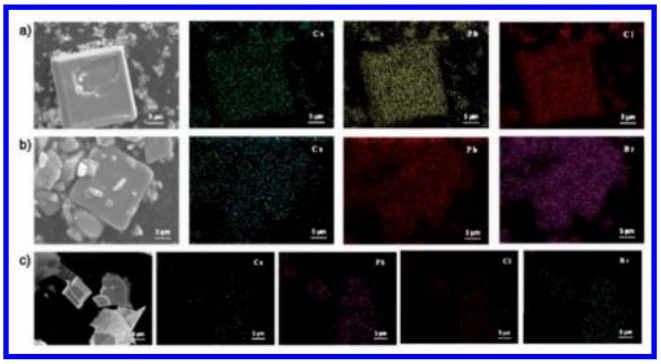

Figure 3. Element mapping images obtained for Cs, Pb, Cl, and Br of selected areas of the (a) $CsPb_2Cl_5$, (b) $CsPb_2Br_5$, and (c) $CsPb_2Cl_2Br_3$ samples.

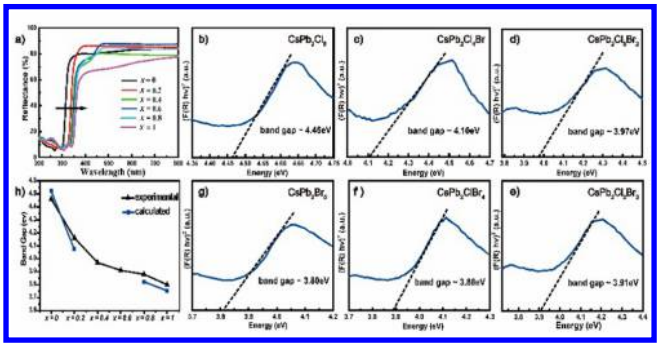

Figure 4. (a) Diffuse-reflectance spectra for $CsPb_2(Cl_{1-x}Br_x)_5$ and the band-gap change map. (b–g) Tauc plots showing the characteristics of the indirect band gap of the $CsPb_2(Cl_{1-x}Br_x)_5$ compounds. (h) Experimental and calculated band-gap values of the $CsPb_2(Cl_{1-x}Br_x)_5$ compounds.

transition, and $F(R_\infty)$ is the Kubelka–Munk function given as[47]

$$F(R_\infty) = (1 - R)^2/2R = K/S \quad (2)$$

where R, K, and S designate the reflection, absorption, and scattering coefficients, respectively. Using the linear extrapolation of $F(R_\infty) \times 2h\nu = 0$, it is possible to estimate the optical band-gap value of a crystal compound. Therefore, the diffuse-reflectance and Tauc plots showing the band-gap characteristics for the $CsPb_2(Cl_{1-x}Br_x)_5$ compounds are shown in Figure 4a–g. In Figure 4a, the trend of the diffuse-reflectance curves for the solid solution $CsPb_2(Cl_{1-x}Br_x)_5$ is basically the same, and the reflectivity increases with increasing wavelength until the peak is reached and it remains unchanged. As x gradually increases, the reflection curve moves toward longer wavelengths. However, the absorption onset is not quite as sharp in the diffuse-reflectance plots. We believe that this change can be attributed to the indirect optical band gap of the materials. It is mentioned in the literature that the lower-energy transition relates to excitation through the band gap, and the higher-energy features appear to be due to exciton transitions from trap states lying above the conduction-band edge.[48] Following this approach, to determine the band gap, we have used the lower absorbance energy onset in the $CsPb_2(Cl_{1-x}Br_x)_5$ compounds, and the values of 4.46, 4.10, 3.97, 3.91, 3.88, and 3.80 eV were obtained for $CsPb_2Cl_5$, $CsPb_2Cl_4Br$, $CsPb_2Cl_3Br_2$, $CsPb_2Cl_2Br_3$, $CsPb_2ClBr_4$, and $CsPb_2Br_5$, respectively. Thus, in the $CsPb_2(Cl_{1-x}Br_x)_5$ compounds, the band gap drastically decreases with increasing Br/Cl ratio.

Band-Structure Calculation. The calculated electronic band structures of the $CsPb_2Cl_5$, $CsPb_2Cl_4Br$, $CsPb_2ClBr_4$, and $CsPb_2Br_5$ compounds are shown in Figure 5a–d. These plots

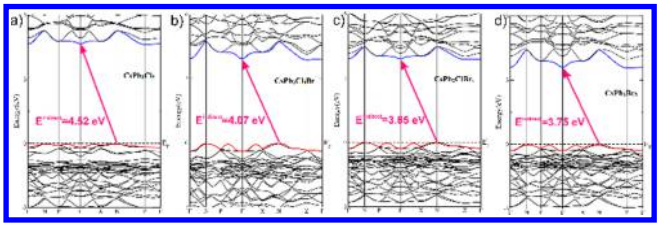

Figure 5. (a–d) Calculated electronic bands of $CsPb_2(Cl_{1-x}Br_x)_5$ (x = 0, 0.2, 0.8, and 1) at the GGA/PBE level.

explore the influence of increasing Br content on the band dispersion. It shows that there is a significant band-gap reduction with increasing Br content. The obtained electronic band structure indicates that the investigated compounds are characterized by the indirect energy band gaps because the location of conduction-band minimum is at the Γ point of the Brillouin zone and the valence-band maximum (VBM) is at the N point of the Brillouin zone. We set the zero point of the energy (Fermi level, EF) at the VBM. It should be pointed out that when x = 0.4 and 0.6, it is difficult to accurately calculate the band gaps because of the complicated occupations of Br and Cl. The calculated band-gap values, in comparison with the experimental results, are shown in Figure 4h and Table 2. As is evident, a very good relationship between the calculated and measured values takes place.

To gain deeper insight into the electronic structure, we have calculated the PDOS for each orbital of the $CsPb_2Cl_5$, $CsPb_2Cl_4Br$, $CsPb_2ClBr_4$, and $CsPb_2Br_5$ compounds, as shown in Figure 6a–h. The calculated DOS confirms our previous result that there is a reduction of the band gap with increasing Br content. It is clear that there is a significant influence of the Br content on the dispersion of each orbital. Also, the composition variation influences hybridization between the orbitals, as is clearly illustrated.

It is interesting to highlight that hybridization may induce the appearance of covalent bonding depending on the degree of hybridization, which is more favorable for the carrier transport than the ionic one.[48] We make use of the calculated PDOS to clarify the chemical-bonding character for these compounds. In the valence bands between −7.0 eV and EF, we have obtained a total number of electrons per electronvolt (e/eV) for each atom orbital in $CsPb_2Cl_5$, $CsPb_2Cl_4Br$, $CsPb_2ClBr_4$, and $CsPb_2Br_5$ as follows: Cs p orbital, 33.0, 33.0, 33.0, and 54 e/eV; Pb s orbital, 3.6, 4.0, 5.4, and 4.3 e/eV; Cl p orbital, 5.2, 3.1, and 4.0 e/eV; Pb p orbital, 1.8, 1.2, 2.0, and 1.5 e/eV; Br p orbital, 3.2, 5.0, and 4.8 e/eV; Pb d orbital, 0.1, 0.75, 0.1, and 0.09 e/eV; Cl s orbital, 0.17, 0.13, and 0.14 e/eV. Thus, following the obtained total number of electrons per electronvolt, one can conclude that some electron density from the Pb, Br, Cs, and Cl atoms is transferred into the valence band and contributes to the covalence interactions between the atoms, according to each atom contribution to the valence band. In the covalence interactions, the strength/weakness arises because of the degree of hybridization and electronegativity differences between the atoms. Respectively, the calculated DOS helps

DOI: 10.1021/acs.inorgchem.8b01572
Inorg. Chem. 2018, 57, 9531–9537

Table 2. Experimental and calculated bandgap values of a $CsPb_2[Cl_{(1-x)}Br_x]_5$ sample

	$x = 0$	$x = 0.2$	$x = 0.4$	$x = 0.6$	$x = 0.8$	$x = 1$
Experimental	4.46 eV	4.10 eV	3.97 eV	3.91 eV	3.88 eV	3.80 eV
Calculated	4.52 eV	4.07 eV			3.85 eV	3.75 eV

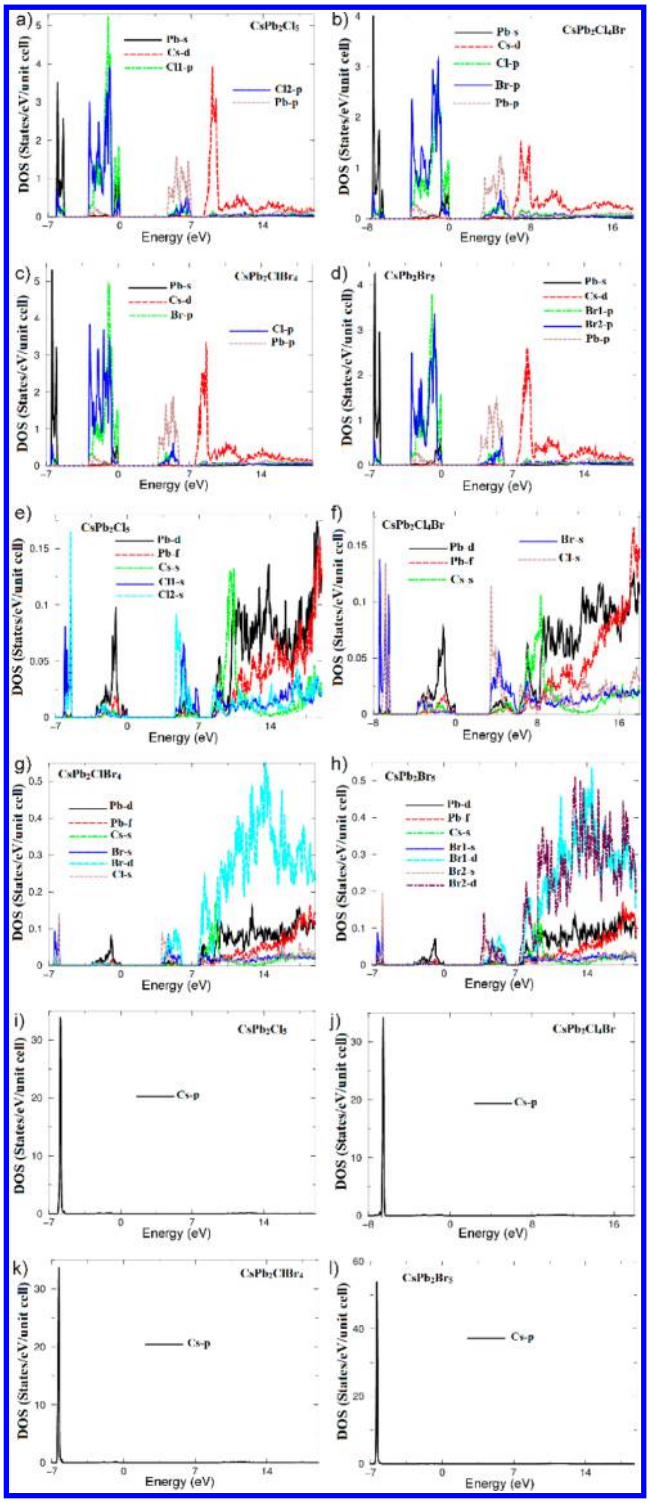

Figure 6. PDOS for each orbital of $CsPb_2(Cl_{1-x}Br_x)_5$ (x = 0, 0.2, 0.8, and 1): $CsPb_2Cl_5$ (a, e, and i), $CsPb_2Cl_4Br$ (b, f, and j), $CsPb_2ClBr_4$ (c, g, and k), and $CsPb_2Br_5$ (d, h, and l) compounds.

us to analyze the nature of the bonds following the classical chemical concept.

CONCLUSIONS

In the present study, 2D halides $CsPb_2(Cl_{1-x}Br_x)_5$ (x = 0, 0.2, 0.4, 0.6, 0.8, and 1) were prepared through the hydrothermal method. The crystal structures of Br-containing compounds were defined for the first time. The optical band gaps of the $CsPb_2(Cl_{1-x}Br_x)_5$ compounds were studied by UV−vis spectroscopy, and it is observed that the band gap can be efficiently tuned via the chemical composition variation. The electronic band-structure calculations reveal that the investigated compounds possess indirect energy band gaps, and this is in a good agreement with the experimental observation. Furthermore, the calculated electronic band structures and DOS confirm our experimental observation that there is a band-gap reduction with increasing Br content. From the calculated PDOS, it is found that some electrons from the Pb, Br, Cs, and Cl atoms were transferred into the valence band, and they contributed to the covalence interactions between the ions. Thus, it can be concluded that the proposed algorithm of the hydrothermal synthesis is universal and it can be applied to different halide solid solutions with Cl/Br substitution, including Rb^+ and Tl^+ compounds. This opens a mechanism for searching new optoelectronic crystalline materials with tunable band gaps.

ASSOCIATED CONTENT

Supporting Information

The Supporting Information is available free of charge on the ACS Publications website at DOI: 10.1021/acs.inorgchem.8b01572.

Figure S1 and Tables S1−S3 (PDF)

AUTHOR INFORMATION

Corresponding Author

*E-mail: xiazg@ustb.edu.cn (Z.X.).

ORCID

Maxim S. Molokeev: 0000-0002-8297-0945
Victor V. Atuchin: 0000-0002-7424-5604
Ali H. Reshak: 0000-0001-9426-8363
Zhiguo Xia: 0000-0002-9670-3223

Notes

The authors declare no competing financial interest.

Further details of the crystal structures of $CsPb_2(Cl_{1-x}Br_x)_5$ (x = 0, 0.2, 0.4, 0.6, 0.8, and 1) may be obtained from Fachinformationszentrum Karlsruhe, 76344 Eggenstein-Leopoldshafen, Germany [fax (+49)7247-808-666; e-mail crystdata@fiz-karlsruhe.de; web page http://www.fiz-karlsruhe.de/request_for_deposited_data.html], quoting the deposition numbers CSD 434748, 434747, 434746, 434745, 434749, and 434744, respectively.

ACKNOWLEDGMENTS

This work was supported by the National Natural Science Foundation of China (Grants 51722202, 91622125, and 51572023) and Natural Science Foundations of Beijing (Grant 2172036). It was also partly developed within the

DOI: 10.1021/acs.inorgchem.8b01572
Inorg. Chem. 2018, 57, 9531−9537

CENTEM project (CZ.1.05/2.1.00/03.0088), cofunded by the ERDF as part of the Ministry of Education, Youth and Sports OP RDI programme, and in the follow-up sustainability stage supported through CENTEM PLUS (LO1402) by the financial means of the Ministry of Education, Youth and Sports under the National Sustainability Programme I. Computational resources were provided by MetaCentrum (LM2010005) and CERIT-SC (CZ.1.05/3.2.00/08.0144) infrastructures. A.H.R. and Z.A.A. extend their appreciation to the International Scientific Partnership Program ISPP at King Saud University for funding this research work through ISPP 0016. This work was partly supported by the Russian Foundation for Basic Research (Grants 16-52-48010 and 17-52-53031). The work was also partly supported by Act 211 Government of the Russian Federation (Contract 02.A03.21.0011). Additionally, the work was partially supported by the Ministry of Education and Science of the Russian Federation (Contract 4.1346.2017/4.6).

REFERENCES

(1) Shi, G. Q.; Wang, Y.; Zhang, F. F.; Zhang, B. B.; Yang, Z.; Hou, X. L.; Pan, S. L.; Poeppelmeier, K. R. Finding the next dee-ultraviolet optical material: $NH_4B_4O_6F$. *J. Am. Chem. Soc.* **2017**, *139*, 10645−10648.

(2) Chen, M. G.; Xia, Z. G.; Molokeev, M. S.; Lin, C. C.; Su, C. C.; Chuang, Y.-C.; Liu, Q. L. Probing Eu^{2+} luminescence from different crystallographic sites in $Ca_{10}M(PO_4)_7$:Eu^{2+} (M = Li, Na, and K) with β-$Ca_3(PO_4)_2$-type structure. *Chem. Mater.* **2017**, *29*, 7563−7570.

(3) Wang, X. F.; Wang, Y.; Zhang, B. B.; Zhang, F. F.; Yang, Z. H.; Pan, S. L. CsB_4O_6F: A congruent-melting deep-ultraviolet nonlinear optical material by combining superior functional units. *Angew. Chem., Int. Ed.* **2017**, *56*, 14119−14123.

(4) Mutailipu, M.; Zhang, M.; Chen, Y.; Lu, X. Q.; Pan, S. L. The structural diversity of halogen-centered secondary building units: Two new mixed-metal borate halides with deep-ultraviolet cut-off edges. *Dalton Trans.* **2017**, *46*, 4923−4928.

(5) Atuchin, V. V.; Subanakov, A. K.; Aleksandrovsky, A. S.; Bazarov, B. G.; Bazarova, J. G.; Gavrilova, T. A.; Krylov, A. S.; Molokeev, M. S.; Oreshonkov, A. S.; Stefanovich, S. Y. Structural and spectroscopic properties of new nonnentrosymmetric self-activated borate $Rb_3EuB_6O_{12}$ wnth B_5O_{10} units. *Mater. Des.* **2018**, *140*, 488−494.

(6) Drokina, T. V.; Petrakovskii, G. A.; Molokeev, M. S.; Velikanov, D. A. Synthesis, crystal structure, and magnetic properties of the $YbFeTi_2O_7$ compound. *Phys. Solid State* **2018**, *60*, 532−536.

(7) Xia, Z. G.; Fang, H. J.; Zhang, X. W.; Molokeev, M. S.; Gautier, R.; Yan, Q. F.; Wei, S. H.; Poeppelmeier, K. R. $CsCu_5Se_3$: A cooper-rich ternary chalcogenide semiconductor with nearly direct band gap for photovoltaic application,. *Chem. Mater.* **2018**, *30*, 1121−1126.

(8) Atuchin, V. V.; Liang, F.; Grazhdannikov, S.; Isaenko, L. I.; Krinitsin, P. G.; Molokeev, M. S.; Prosvirin, I. P.; Jiang, X. X.; Lin, Z. S. Negative thermal expansion and electronic structure variation of chalcopyrite type $LiGaTe_2$. *RSC Adv.* **2018**, *8*, 9946−9955.

(9) Liu, Y.; Molokeev, M. S.; Liu, Q. L.; Xia, Z. G. Crystal structures, phase transitions and thermal expansion properties of $NaZr_2(PO_4)_3$-$SrZr_4(PO_4)_6$ solid solutions. *Inorg. Chem. Front.* **2018**, *5*, 619−625.

(10) Garg, V.; Sengar, B. S.; Awasthi, V.; Kumar, A.; Singh, R.; Kumar, S.; Mukherjee, C.; Atuchin, V. V.; Mukherjee, S. Investigation of dual-ion beam sputter-instigated pkasmon generation in TCOs: A case study of GZO. *ACS Appl. Mater. Interfaces* **2018**, *10*, 5464−5474.

(11) Jiang, X. X.; Yang, Y.; Molokeev, M. S.; Gong, P.; Liang, F.; Wang, S. H.; Liu, L.; Wu, X.; Li, X. D.; Li, Y. C.; Wu, S. F.; Li, W.; Wu, Y. C.; Lin, Z. S. Zero linear compressibility in nondense borates with a "Lu-Ban stool"-like structure. *Adv. Mater.* **2018**, 1801313.

(12) Nedelcu, G.; Protesescu, L.; Yakunin, S.; Bodnarchuk, M. I.; Grotevent, M. J.; Kovalenko, M. V. Fast anion-exchange in highly luminescent nanocrystals of cesium lead halide perovskites ($CsPbX_3$, X= Cl, Br, I). *Nano Lett.* **2015**, *15*, 5635−5640.

(13) Akkerman, Q. A.; D'Innocenzo, V.; Accornero, S.; Scarpellini, A.; Petrozza, A.; Prato, M.; Manna, L. Tuning the optical properties of cesium lead halide perovskite nanocrystals by anion exchange reactions. *J. Am. Chem. Soc.* **2015**, *137*, 10276−10281.

(14) Yakunin, S.; Protesescu, L.; Krieg, F.; Bodnarchuk, M. I.; Nedelcu, G.; Humer, M.; De Luca, G.; Fiebig, M.; Heiss, W.; Kovalenko, M. V. Low-threshold amplified spontaneous emission and lasing from colloidal nanocrystals of caesium lead halide perovskites. *Nat. Commun.* **2015**, *6*, 8056.

(15) Yassitepe, E.; Yang, Z.; Voznyy, O.; Kim, Y.; Walters, G.; Castañeda, J. A.; Kanjanaboos, P.; Yuan, M.; Gong, X.; Fan, F.; Pan, J.; Hoogland, S.; Comin, R.; Bakr, O. M.; Padilha, L. A.; Nogueira, A. F.; Sargent, E. H. Amine-Free Synthesis of Cesium Lead Halide Perovskite Quantum Dots for Efficient Light-Emitting Diodes. *Adv. Funct. Mater.* **2016**, *26*, 8757−8763.

(16) Quan, L. N.; Quintero-Bermudez, R.; Voznyy, O.; Walters, G.; Jain, A.; Fan, J. Z.; Zheng, X.; Yang, Z.; Sargent, E. H. Highly Emissive Green Perovskite Nanocrystals in a Solid State Crystalline Matrix. *Adv. Mater.* **2017**, *29*, 1605945.

(17) Nikl, M.; Nitsch, K.; Chval, J.; Somma, F.; Phani, A.; Santucci, S.; Giampaolo, C.; Fabeni, P.; Pazzi, G.; Feng, X. Optical and structural properties of ternary nanoaggregates in CsI-PbI_2 co-evaporated thin films. *J. Phys.: Condens. Matter* **2000**, *12*, 1939.

(18) Mitolo, D.; Pinto, D.; Garavelli, A.; Bindi, L.; Vurro, F. The role of the minor substitutions in the crystal structure of natural challacolloite, KPb_2Cl_5, and hephaistosite, $TlPb_2Cl_5$, from Vulcano (Aeolian Archipelago, Italy). *Mineral. Petrol.* **2009**, *96*, 121−128.

(19) Atuchin, V.; Isaenko, L.; Kesler, V.; Tarasova, A. Y. Single crystal growth and surface chemical stability of KPb_2Br_5. *J. Cryst. Growth* **2011**, *318*, 1000−1004.

(20) Bekenev, V.; Khyzhun, O. Y.; Sinelnichenko, A.; Atuchin, V.; Parasyuk, O.; Yurchenko, O.; Bezsmolnyy, Y.; Kityk, A.; Szkutnik, J.; Całus, S. Crystal growth and the electronic structure of Tl_3PbCl_5. *J. Phys. Chem. Solids* **2011**, *72*, 705−713.

(21) Atuchin, V.; Isaenko, L.; Kesler, V.; Pokrovsky, L.; Tarasova, A. Y. Electronic parameters and top surface chemical stability of $RbPb_2Br_5$. *Mater. Chem. Phys.* **2012**, *132*, 82−86.

(22) Tarasova, A. Y.; Isaenko, L.; Kesler, V.; Pashkov, V.; Yelisseyev, A.; Denysyuk, N.; Khyzhun, O. Y. Electronic structure and fundamental absorption edges of KPb_2Br_5, $K_{0.5}Rb_{0.5}Pb_2Br_5$, and $RbPb_2Br_5$ single crystals. *J. Phys. Chem. Solids* **2012**, *73*, 674−682.

(23) Ithurria, S.; Tessier, M.; Mahler, B.; Lobo, R.; Dubertret, B.; Efros, A. L. Colloidal nanoplatelets with two-dimensional electronic structure. *Nat. Mater.* **2011**, *10*, 936.

(24) Tang, X.; Hu, Z.; Yuan, W.; Hu, W.; Shao, H.; Han, D.; Zheng, J.; Hao, J.; Zang, Z.; Du, J.; Leng, Y.; Fang, L.; Zhou, M. Perovskite $CsPb_2Br_5$ microplate laser with enhanced stability and tunable properties. *Adv. Opt. Mater.* **2017**, *5*, 1600788.

(25) Han, C.; Li, C.; Zang, Z.; Wang, M.; Sun, K.; Tang, X.; Du, J. Tunable luminescent $CsPb_2Br_5$ nanoplatelets: applications in light-emitting diodes and photodetectors. *Photonics Res.* **2017**, *5*, 473−480.

(26) Tang, X.; Han, S.; Zu, Z.; Hu, W.; Zhou, M.; Du, J.; Hu, Z.; Li, S.; Zang, Z. All-Inorganic Perovskite $CsPb_2Br_5$ Microsheets for Photodetector Application. *Front. Phys.* **2018**, *5*, 69.

(27) Lv, J.; Fang, L.; Shen, J. Synthesis of highly luminescent $CsPb_2Br_5$ nanoplatelets and their application for light-emitting diodes. *Mater. Lett.* **2018**, *211*, 199−202.

(28) Kim, M. K.; Jo, V.; Ok, K. M. New Variant of Highly Symmetric Layered Perovskite with Coordinated NO_3^- Ligand: Hydrothermal Synthesis, Structure, and Characterization of $Cs_2PbCl_2(NO_3)_2$. *Inorg. Chem.* **2009**, *48*, 7368−7372.

(29) Dursun, I.; De Bastiani, M.; Turedi, B.; Alamer, B.; Shkurenko, A.; Yin, J.; El-Zohry, A. M.; Gereige, I.; AlSaggaf, A.; Mohammed, O. F.; Eddaoudi, M.; Bakr, O. M. $CsPb_2Br_5$ single crystals synthesis and characterization. *ChemSusChem* **2017**, *10*, 3746−3749.

(30) Boese, R.; Blaeser, D.; Hueben, W. Crystal structure of silver dilead pentabromide. *Z. Kristallogr.* **1990**, *191*, 135−136.

DOI: 10.1021/acs.inorgchem.8b01572
Inorg. Chem. 2018, 57, 9531−9537

(31) Merkulov, A.; Isaenko, L.; Pashkov, V.; Mazur, V.; Virovets, A.; Naumov, D. Y. Crystal structure of KPb_2Cl_5 and KPb_2Br_5. *J. Struct. Chem.* **2005**, *46*, 103−108.
(32) Velázquez, M.; Ferrier, A.; Pérez, O.; Péchev, S.; Gravereau, P.; Chaminade, J. P.; Moncorgé, R. A Cationic Order-Disorder Phase Transition in KPb_2Cl_5. *Eur. J. Inorg. Chem.* **2006**, *2006*, 4168−4178.
(33) Keller, H.-L. Notiz zur Kristallstruktur von APb_2Cl_5-Verbindungen/Notice about Crystal Structures of APb_2Cl_5-Compounds. *Z. Naturforsch. B* **1976**, *31*, 885−885.
(34) Powell, H.; Tasker, H. The valency angle of bivalent lead: the crystal structure of ammonium, rubidium, and potassium pentabromodiplumbites. *J. Chem. Soc.* **1937**, *25*, 119−123.
(35) Campostrini, I.; Demartin, F.; Gramaccioli, C. M.; Orlandi, P. Hephaistosite, $TlPb_2Cl_5$, a new thallium mineral species from La Fossa crater, Vulcano, Aeolian Islands, Italy. *Can. Mineral.* **2008**, *46*, 701−708.
(36) Becker, D.; Beck, H. P. High Pressure Study of $NH_4Pb_2Br_5$ Type Compounds. I structural parameters and their evolution under high pressure. *Z. Anorg. Allg. Chem.* **2004**, *630*, 1924−1932.
(37) *TOPASV4: General Profile and Structure Analysis Software for Powder Diffraction Data, User's Manual*; Bruker AXS: Karlsruhe, Germany, 2008.
(38) Blaha, P.; Schwarz, K.; Madsen, G.; Kvasnicka, D.; Luitz, J. *WIEN2K, An augmented plane wave+ local orbitals program for calculating crystal properties*; Vienna University of Technology: Vienna, Austria, 2001.
(39) Tran, F.; Blaha, P. Accurate band gaps of semiconductors and insulators with a semilocal exchange-correlation potential. *Phys. Rev. Lett.* **2009**, *102*, 226401.
(40) Blöchl, P. E.; Jepsen, O.; Andersen, O. K. Improved tetrahedron method for Brillouin-zone integrations. *Phys. Rev. B: Condens. Matter Mater. Phys.* **1994**, *49*, 16223.
(41) Kuznetsova, I. Y.; Kovaleva, I.; Fedorov, V. Interaction of lead bromide with cesium and cadmium bromides. *Russ. J. Inorg. Chem.* **2001**, *46*, 1900−1905.
(42) Brese, N.; O'keeffe, M. Bond-valence parameters for solids. *Acta Crystallogr., Sect. B: Struct. Sci.* **1991**, *47*, 192−197.
(43) Atuchin, V.; Chimitova, O.; Gavrilova, T.; Molokeev, M.; Kim, S.-J.; Surovtsev, N.; Bazarov, B. Synthesis, structural and vibrational properties of microcrystalline $RbNd(MoO_4)_2$. *J. Cryst. Growth* **2011**, *318*, 683−686.
(44) Kokh, K. A.; Atuchin, V.; Gavrilova, T.; Kuratieva, N.; Pervukhina, N.; Surovtsev, N. Microstructural and vibrational properties of PVT grown Sb_2Te_3 crystals. *Solid State Commun.* **2014**, *177*, 16−19.
(45) Atuchin, V. V.; Beisel, N. F.; Galashov, E. N.; Mandrik, E. M.; Molokeev, M. S.; Yelisseyev, A. P.; Yusuf, A. A.; Xia, Z. Pressure-stimulated synthesis and luminescence properties of microcrystalline $(Lu, Y)_3Al_5O_{12}:Ce^{3+}$ garnet phosphors. *ACS Appl. Mater. Interfaces* **2015**, *7*, 26235−26243.
(46) Atuchin, V.; Isaenko, L.; Kesler, V.; Lin, Z.; Molokeev, M.; Yelisseyev, A.; Zhurkov, S. Exploration on anion ordering, optical properties and electronic structure in $K_3WO_3F_3$ elpasolite. *J. Solid State Chem.* **2012**, *187*, 159−164.
(47) Xia, Z.; Zhang, Y.; Molokeev, M. S.; Atuchin, V. V. Structural and luminescence properties of yellow-emitting $NaScSi_2O_6:Eu^{2+}$ phosphors: Eu^{2+} site preference analysis and generation of red emission by codoping Mn^{2+} for white-light-emitting diode applications. *J. Phys. Chem. C* **2013**, *117*, 20847−20854.
(48) Wu, F.; Song, H.; Jia, J.; Hu, X. Effects of Ce, Y, and Sm doping on the thermoelectric properties of Bi_2Te_3 alloy. *Prog. Nat. Sci.* **2013**, *23*, 408−412.

DOI: 10.1021/acs.inorgchem.8b01572
Inorg. Chem. 2018, 57, 9531−9537